The Low-Level Jet as a Western Boundary Current

DAVID L. T. ANDERSON

Department of Applied Mathematics and Theoretical Physics, Cambridge University, Cambridge, England

(Manuscript received 23 December 1975, in revised form 12 April 1976)

ABSTRACT

The low-level jet which flows across the equator and up the Somali coast is considered as a western boundary current of the East African mountain chain. The jet is assumed to be forced by the low-level divergence in the subtropical high pressure belt of the Southern Hemisphere and convergence in the monsoon trough. A simple model with this type of forcing is proposed and analytic and numerical solutions obtained. These appear to be in reasonable agreement with observation. The sensitivity of the model jet to spatial variation in the forcing, temporal changes in the intensity of the low-level convergence, and nonlinearity are examined.

1. Introduction

During the southwest monsoon an intense low-level jet has been observed (Findlater, 1974) which flows across the equator carrying Southern Hemisphere air northward up the African continent. At about 10°N this jet breaks away from the land and heads eastward (Fig. 1a). At the location where the jet passes over the ocean there is strong coastal upwelling and thus it is likely that this jet plays an important role in the seasonal development of the Somali Current (Anderson and Rowlands, 1976b), an intense ocean current which flows northward only during the southwest monsoon but whose strength then is comparable with that of the Gulf Stream. Thus the mechanisms forcing and controlling this jet are of interest to oceanographers. In fact, the low-level atmospheric jet may be formed by one of the mechanisms which gives rise to the Somali Current: concentration of long planetary waves by meridional boundaries (Lighthill, 1969). Fig. 1b (from Findlater, 1974) emphasize the importance of the mountains in the location of the low-level jet.[1] Velocities in the jet core are ~ 15 m s^{-1} when averaged over the month of July but much higher velocities are often obtained [up to 50 m s^{-1} (Findlater, 1974)]. The low-level jet is also of meteorological interest in its own right because within a zone of less than 2% of the total equatorial circumference, almost 50% of the total cross-equatorial transport is achieved (Rao, 1964).

The overall flow patterns and surface pressure pattern for July are given in Figs. 3.1 and 3.2 of Hahn and Manabe (1975). To the south, centered at ~ 30°S and spanning a wide band of longitudes, is the high pressure belt of the Southern Hemisphere, while to the north is the monsoon trough and heat low over India, Iran and Arabia. The fact that the core of the low-level jet is centered at as low a level as 870 mb compared with more typical jet core levels (200–300 mb) allows us to analyze its behavior with a simple model. The main physical processes required to explain this jet are considered to be 1) a region of inflow at ~ 30°S representing the low-level divergence associated with the Southern Hemisphere high pressure belt, 2) a region of outflow at ~ 30°N representing the low-level convergence of the monsoon trough, and 3) a partial or complete north-south barrier spanning the equator and representing the mountain ranges of East Africa.

In considering the flow to be controlled by the mid-latitude distribution of divergence/convergence,[2] we are assuming that the effect of the large-scale circulation of the atmosphere on this distribution is more important than that of the local low-level circulation. Hahn and Manabe (1975) have shown that the absence of mountains disturbs the region of low-level convergence, but this is presumably due more to the local action of the Himalayas than to the remote effect of the East African mountain chain perturbing the low-level flow field and so producing a different convergence pattern over India. Further, although large-scale Ekman pumping in the lowest 200 mb by the mid-tropospheric circulation must be acknowledged as possible, since no evidence appears to exist to support or refute the idea, we will ignore it and consider the integrated effect of the lowest 200 mb.

In the following section, a simple linear model will be formulated. Solutions will first be given in the absence of boundaries, and then the temporal evolution of the flow in the presence of a boundary will be developed. This leads us to consider the frictional boundary layer

[1] The similarity between western oceanic boundary currents and atmospheric jets has previously been discussed by Newton (1959) and Wexler (1961) for the low-level jet east of the Rockies.

[2] Source/sink flow in a rotating fluid has also been considered by Hide (1968).

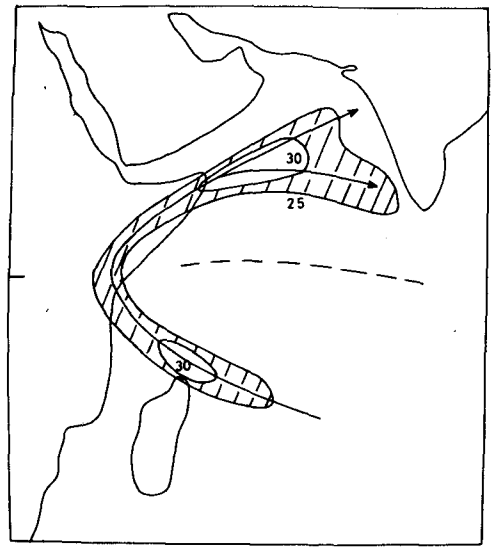

FIG. 1a. Monthly mean air flow at 1 km in July showing the major axis of the low-level jet. Velocities are in knots. Dashed line indicates axis of minimum wind. [Redrawn from Findlater (1974).]

solution. In Section 3, numerical solutions will be obtained.

2. Formulation

For this analysis we consider the atmosphere to be split into two layers (of densities ρ_1, ρ_2) roughly say at the level of the trade wind inversion. The upper layer will then act mainly to reduce the effect of gravity on the lower layer, by a factor $g'/g=-(\rho_2-\rho_1)/\rho_1$, and give the lower layer an effective depth $H=H_1H_2/(H_1+H_2)$, where H_1 and H_2 are the mean depths of the two layers and $H_2\approx 4H_1$ if the upper layer is considered incompressible. In Fig. 2 potential temperature is plotted as a function of pressure for the tropical atmosphere, and the mean value used when the atmosphere is considered split into two levels is shown. This gives a value for $g'\approx g/20$. In fact, results are not very sensitive to this parameter because (as shown later) it occurs only as the $\frac{1}{4}$ power in scaling length and time, or the $\frac{1}{2}$ power is scaling velocity.

For simplicity, we shall consider an equatorial β-plane for which $f=\beta y$. Then the linearized, free-surface equations are

$$\left.\begin{aligned} u_t-fv&=-p_x/\rho=-g'hx\\ v_t+fu&=-p_y/\rho=-g'hy\\ h_t+H(u_x+v_y)&=Q \end{aligned}\right\}, \tag{1}$$

where H is the effective mean depth of the fluid, h the perturbation depth, and Q the source/sink term.

As mentioned earlier, if the large-scale mid-tropospheric pumping is important, then h is not a free parameter. Further, even in the absence of such pumping it is not clear whether a free surface or a rigid lid is the most appropriate model (i.e., whether h_t is a free variable or is zero). However, since in general only the effect of long planetary waves is important and not the method by which these waves produce their effect, little difference is likely in the long-term solution, particularly since, it will be argued, this is likely to be frictionally dominated.

We define nondimensional quantities

$$\left.\begin{aligned} x^*&=\frac{(2\beta)^{\frac{1}{2}}}{(g'H)^{\frac{1}{4}}}x,\quad t^*=(2\beta)^{\frac{1}{2}}(g'H)^{\frac{1}{4}}t\\ v^*&=v/(g'H)^{\frac{1}{2}},\quad h^*=h/H,\quad Q^*=Q/[(2\beta)^{\frac{1}{2}}(g'H)^{\frac{1}{4}}H] \end{aligned}\right\}. \tag{2}$$

Hence, dropping the asterisks, we have

$$u_t-\tfrac{1}{2}yv=-h_x, \tag{3a}$$

$$v_t+\tfrac{1}{2}yu=-h_y, \tag{3b}$$

$$h_t+u_x+v_y=Q. \tag{3c}$$

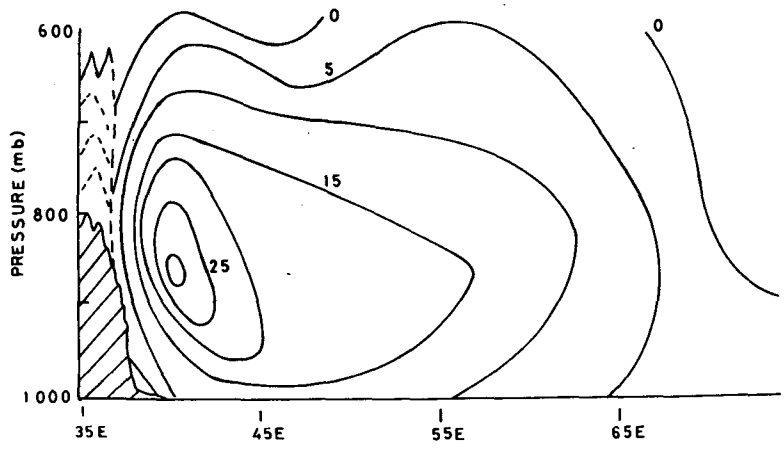

FIG. 1b. Vertical section along the equator of the meridional wind in July showing the cross-equatorial jet and its proximity to the mountains. Velocities are in knots. [Redrawn from Findlater (1974).]

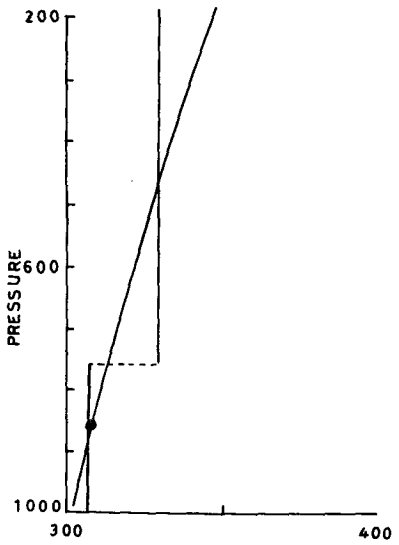

FIG. 2. Potential temperature (φ) as a function of pressure (mb) for the tropical atmosphere. For a two-level atmosphere, mean values of φ are 309 and 328K which gives $g'/g=(\varphi_2-\varphi_1)/\varphi_2\approx 1/20$.

From Findlater (1974), the depth of the jet is ~ 2 km with the core at $\sim 1\frac{1}{2}$ km, so we will take $H_1=2$ km, $\rho=1.3$ kg m^{-3}, $\beta=2\times 10^{-11}$ m^{-1} s^{-1}, whence nondimensional units of distance, time and velocity correspond to 1000 km, 0.3 day and 30 m s^{-1}, respectively.

Before considering the general solution to (3) in the presence of meridional boundaries, it is instructive to examine the solution in the absence of boundary influences, where a simple solution is possible. Boundary effects are then considered in Sections 2b and 2c.

a. Simple solutions to (3) when there are no x variations in the forcing and no boundary effects

The equations are now

$$u_t=\tfrac{1}{2}yv, \tag{4a}$$

$$v_t=-\tfrac{1}{2}yu-h_y, \tag{4b}$$

$$h_t=Q-v_y. \tag{4c}$$

Eliminating h and u in favor of v gives

$$-v_{tt}+v_{yy}-\tfrac{1}{4}y^2v=Q_y. \tag{5}$$

The structure of this equation shows the presence of inertial oscillations, whose presence in a linear flow is not likely to be significant in the mean flow pattern. Excluding such oscillations, v is the solution of

$$v_{yy}-\tfrac{1}{4}y^2v=Q_y. \tag{6}$$

Having solved for v, u can be calculated from (4a). The interesting result here is that the spatial distribution of streamlines of the flow is independent of Q (though the direction of flow and intensity are not). This follows from (4a) for

$$u/v=\frac{dx}{dy}=\tfrac{1}{2}yt,$$

i.e.,

$$x=y^2t/4. \tag{7}$$

This is the equation of a parabola (which expands for increasing t), since u increases linearly with time while v is independent of time. This means that in the absence of any meridional boundary or spatial inhomogeneities of Q, the fluid emerging from the high pressure belts of

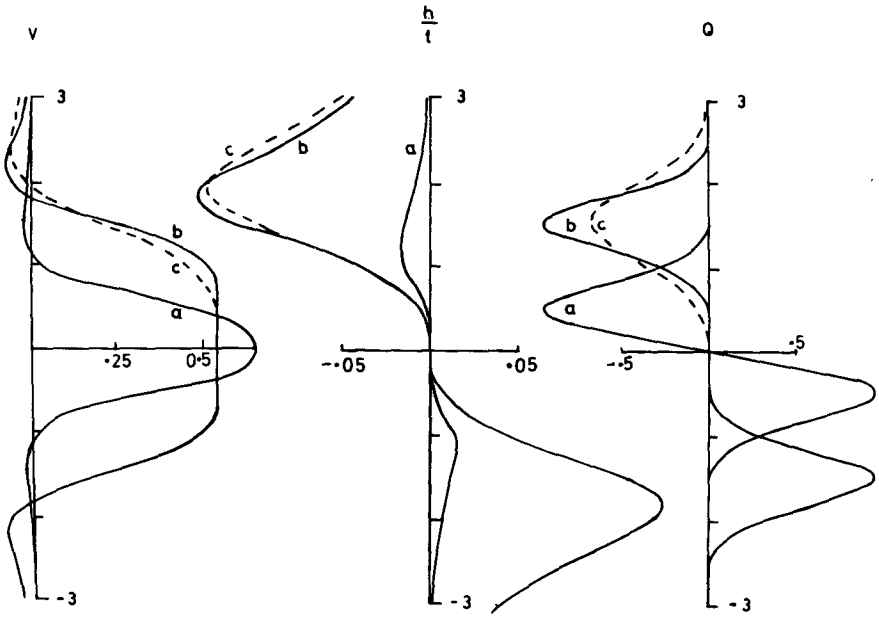

FIG. 3. Plots of v, h/t and Q as function of y for Q defined by Eqs. (8a), (8b) and (8c), respectively.

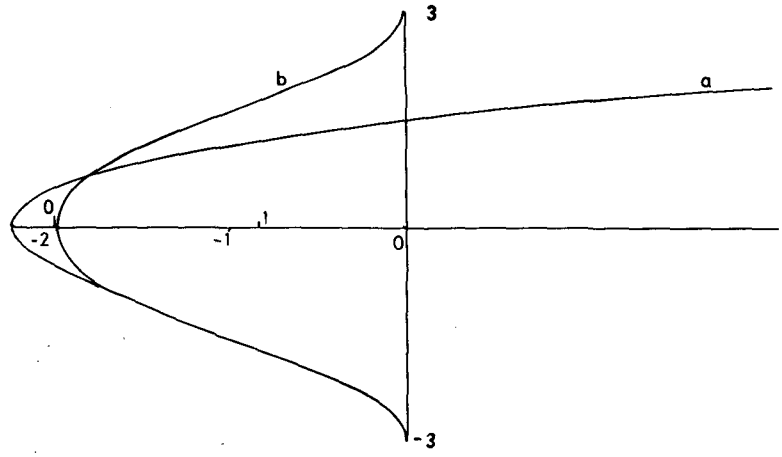

FIG. 4. Curve a is a plot of the trajectory of an air particle in the inviscid case emitted at $y=-3$. It travels downstream before crossing the equator and heading for the sink at $y=+3$. The zonal velocity increases linearly with time so it returns eastward faster than it went westward. The trajectory is plotted in (v_0x,y) space (lower scale). Curve b shows the trajectory of an air parcel in the viscous case, plotted in (Kx,y) space (upper scale).

the Southern Hemisphere will travel a long way downstream before crossing the equator and heading for the fluid sink of the Northern Hemisphere. In Fig. 3, v, h/t and Q are plotted for three different distributions of Q. These are

$$Q=\exp[-5(y+y_0)^2]-\exp[-5(y-y_0)^2], \quad y_0=0.5, \quad (8a)$$

$$Q=\exp[-5(y+y_0)^2]-\exp[-5(y-y_0)^2], \quad y_0=1.5, \quad (8b)$$

$$Q=\exp[-5(y+y_0)^2]-2^{-\frac{1}{2}}\exp[-2.5(y-y_0)^2], \quad y_0=1.5. \quad (8c)$$

Expressions (8a) and (8b) differ only in that the source/sink distribution is further from the equator in (b) than in (a), while (8c) has the sink of equal total strength to (b) but spread out over a larger latitude band. Solutions (8b) and (8c) differ only in the region where the forcing is different, i.e., a change in the source or sink distribution in one hemisphere does not perturb the flow in the other. When the source/sink distribution is distinct from the equator, the north-south flow is essentially constant over a broad band of latitude (cf. curves b, c in Fig. 3). For a source/sink distribution for which $v=v_0=$ constant in the range $-y_0<y<y_0$, the trajectories are given by $y=-y_0+v_0t$, $x=v_0^2t^3/6-y_0v_0t^2/4$. For the case $y_0=3$, this trajectory is plotted in Fig. 4a in (xv_0,y) space. The asymmetry in the trajectory results from the fact that as the particle is traveling northward the zonal velocities are increasing with time and thus the particle can return eastward faster than it went westward.

The monotonic increase in zonal velocity will lead to frictional or inertial forces becoming important factors. For a frictionless fluid, a steady-state nonlinear solution is possible with $v=\int Q\partial y$, $u=\frac{1}{4}y^2+u_0$, the nonlinear terms changing the parity of the u solution compared to that above. If damping is included in the form of an eddy diffusivity of momentum, then a linear steady-state solution is possible with $v=\int Q\partial y$ as before. For a δ-function source/sink at $y=\pm y_0$, the velocity will be constant, equal to v_0 in the range $-y_0<y<y_0$ and the streamlines or trajectories given by $Kx=-y^4/48+y_0^2y^2/24$ are plotted in Fig. 4b.

b. The solution in the presence of a north-south wall

In this section the dynamical effects of inserting a wall at $x=0$ will be examined. For a frictionless fluid it will be shown that there is no steady solution. Instead a jet will form at the boundary and the width of this jet will continue to decrease indefinitely (Lighthill, 1969; Anderson and Gill, 1975). This will in turn imply that dissipative and/or nonlinear processes will become important. The effect of both of these processes will then be examined; dissipative effects in Section 2c and nonlinear as well as spatial inhomogeneities in Section 3. Eqs. (3) can be rewritten as

$$q_t+q_x+\left(\frac{\partial}{\partial y}-\tfrac{1}{2}y\right)v=Q(x,y,t), \quad (9a)$$

$$r_t-r_x+\left(\frac{\partial}{\partial y}+\tfrac{1}{2}y\right)u=Q(x,y,t), \quad (9b)$$

$$2v_t+\left(\frac{\partial}{\partial y}+\tfrac{1}{2}y\right)q+\left(\frac{\partial}{\partial y}-\tfrac{1}{2}y\right)r=0, \quad (9c)$$

where $q=h+u$, $r=h-u$ (Gill and Clarke, 1974).

The operators $[(\partial/\partial y)\pm\frac{1}{2}y)]$ are the raising and lowering ladder operators of the parabolic cylinder

functions (Lighthill, 1969); thus it is convenient to expand q, r, v, etc. as series of parabolic cylinder functions, e.g.,

$$q=\sum_{m=0}^{\infty} q^m(x,t)D_m(y),$$

where $D_m(y)$ is the mth parabolic cylinder function of Whittaker.

Then equations for q^m, r^m, v^m can be written as (Anderson and Rowlands, 1976a)

$$\left.\begin{aligned}
&2q^{m+1}_{tt}-2q^{m+1}_{xxt}+(2m+1)q^{m+1}_t-q^{m+1}_x\\
&\quad=2Q^{m+1}_{tt}-2Q^{m+1}_{xt}+mQ^{m+1}+Q^{m-1}\\
&2r^{m-1}_{tt}-2r^{m-1}_{xxt}+(2m+1)r^{m-1}_t-r^{m-1}_x\\
&\quad=2Q^{m-1}_{tt}+2Q^{m-1}_{xt}\\
&\qquad+m(m+1)Q^{m+1}+(m+1)Q^{m-1}\\
&2v^m_{tt}-2v^m_{xxt}+(2m+1)v^m_t-v^m_x\\
&\quad=-(m+1)Q^{m+1}_t\\
&\qquad+(m+1)Q^{m+1}_x+Q^{m-1}_t+Q^{m-1}_x
\end{aligned}\right\}. \tag{10}$$

For a western boundary, the boundary condition $u=0$ is most conveniently expressed as (Anderson and Rowlands, 1976b)

$$\left.\begin{aligned}
r^{m-1}&=q^{m-1}\\
2r^{m-1}_{tt}-2r^{m-1}_{xt}-m(m+1)r^{m+1}+mr^{m-1}&=2Q^{m-1}_t
\end{aligned}\right\}. \tag{11}$$

The low-order members to the sequence (10) are

$$\left.\begin{aligned}
q^0_t+q^0_x&=Q^0\\
2q^1_{tt}+2q^1_{xt}+q^1&=2Q^1_t
\end{aligned}\right\}. \tag{12}$$

The solutions to (10), (11) and (12) are obtained by taking Laplace transforms, where $\hat{q}$ is the Laplace transform with respect to t of the variable q, i.e.,

$$\hat{q}=\int_0^{\infty} qe^{-st}dt.$$

The solution of the Laplace transform of Eqs. (10)–(12) is

$$\left.\begin{aligned}
\hat{r}^{m-1}&=A^{m-1}\exp(k^{m-1}x)+I^{m-1}\\
\hat{q}^{m+1}&=B^{m+1}\exp(k^{m-1}x)+J^{m+1}\\
k^{m-1}&=\{-1-[1+16(m+\tfrac{1}{2})s^2+16s^4]^{\frac{1}{2}}\}/4s
\end{aligned}\right\}, \tag{13}$$

and I^{m-1}, J^{m+1} are particular integrals of (10). For a source distribution independent of x, I^{m-1}, J^{m+1} can be expressed as

$$\left.\begin{aligned}
I^{m-1}&=\frac{s\hat{Q}^{m-1}+[m(m+1)\hat{Q}^{m+1}+(m+1)\hat{Q}^{m-1}]/2s}{(m+\frac{1}{2}+s^2)}\\
J^{m+1}&=\frac{s\hat{Q}^{m+1}+(m\hat{Q}^{m+1}+\hat{Q}^{m-1})/2s}{(m+\frac{1}{2}+s^2)}
\end{aligned}\right\}. \tag{14}$$

As a result, from (11), we have

$$\left.\begin{aligned}
A^{m-1}&=\frac{-(2s^2+m)I^{m-1}+2s\hat{Q}^{m-1}+m(m+1)\hat{r}^{m+1}_{x=0}}{(2s^2-2sk^{m-1}_r+m)}\\
B^{m+1}&=A^{m+1}+I^{m+1}-J^{m+1}
\end{aligned}\right\}. \tag{15}$$

The solution for r, and by a similar method for q, can be obtained using the techniques outlined in Anderson and Rowlands (1976a), but it is more convenient to examine the long-term solution for q, r, v when a much simpler and informative approximate analytic solution can be obtained. The asymptotic solution for this case is obtained by letting $s\to 0$. Then

$$\left.\begin{aligned}
A^{m-1}&\to\frac{-mI^{m-1}+m(m+1)\hat{r}^{m+1}_{x=0}}{(m+1)}\\
I^{m-1}&\to\frac{m(m+1)\hat{Q}^{m+1}+(m+1)\hat{Q}^{m-1}}{2s(m+\frac{1}{2})}
\end{aligned}\right\}. \tag{16}$$

For a steady source/sink distribution, applied at $t=0$, $\hat{Q}^{m+1}=Q^{m+1}/s$ and hence

$$\hat{r}=\frac{F_1(y)e^{-x/2s}+G_1(y)}{s^2}, \tag{17}$$

where

$$\left.\begin{aligned}
F_1(y)&=\sum_{m=0}^{\infty} s^2A^mD_m(y)\\
G_1(y)&=\sum_{m=0}^{\infty} s^2I^mD_m(y)
\end{aligned}\right\}.$$

This implies r has an asymptotic solution of the form

$$r=F_1(y)\left(\frac{2t}{x}\right)^{\frac{1}{4}}J_1(\sqrt{2xt})+G_1(y)t. \tag{18}$$

The solution for q follows the same pattern except that the lowest member, the Kelvin wave, has to be treated differently. Since the Kelvin wave solution is $q^0(t)=r^0_{x=0}(t-x)H(t-x)+Q^0t$, the solution for q is of the form

$$q=F_2(y)\left(\frac{2t}{x}\right)^{\frac{1}{4}}J_1(\sqrt{2xt})+G_2(y)t+q^0(t)D_0(y), \tag{19}$$

where

$$F_2(y)=\sum_{m=1}^{\infty} s^2B^mD_m(y),\quad G_2(y)=\sum_{m=1}^{\infty} s^2J^mD_m(y),$$

and J_1 is a Bessel function of order 1. The solution for v can be obtained from the asymptotic form of the Laplace transform of the spectral form of (9c) which is

$$2s\hat{v}^m=-(m+1)\hat{q}^{m+1}+\hat{r}^{m-1}. \tag{20}$$

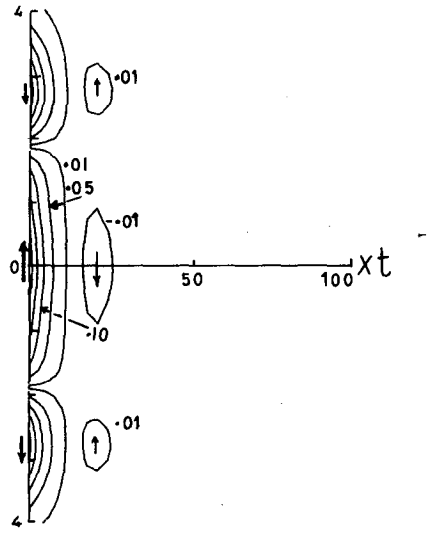

FIG. 5a. Contours of the asymptotic meridional velocity s/t^2 as a function of y and xt for the dynamic spin-up phase showing the strong boundary currents. There are in addition weak flow reversals associated with the zeros of the Bessel function $J_2(\sqrt{2xt})$ [Eq. (22)]. The contour interval is 0.05, except that the 0.01 contour is also drawn to indicate the weak reverse circulations. The interior velocity field is not included (see text, Section 2b).

This will not give the correct interior solution for v, however, as asymptotically $(m+1)\hat{q}^{m+1}=\hat{r}^{m-1}$ in the interior $[(m+1)J^{m+1}=I^{m-1}]$, i.e., to leading order the right-hand side of (20) is zero. In fact, we know from (10) that v is constant in the interior. However, the boundary solution for v is correctly given by (20) and hence $\hat{v}$ is of the form $e^{-x/2s}F_3(y)/s^3+G_3(y)/s$ implying that v is of the form

$$v=F_3(y)\frac{2t}{x}J_2(\sqrt{2xt})+G_3(y). \tag{21}$$

For "large" times, the boundary response near the coast dominates over the interior solution and we have

$$v/t^2=\frac{2F_3(y)}{xt}J_2(\sqrt{2xt}). \tag{22}$$

This solution for v/t^2 is plotted as a function of xt in Fig. 5a and u/t is plotted in Fig. 5b, for the forcing of the form

$$Q=\left\{\begin{matrix}-1, & 2.3<x<3\\ +1, & -3<x<-2.3\end{matrix}\right\}, \tag{23}$$

which corresponds to low-level convergence/divergence in the range of 23° to 30°. There is a strong jet near the boundary quickly becoming small in the interior, with weak southerly, then northerly flow regions. These flow reversals show the zeros of the Bessel function J_3. The interior flow for v has not been included. Note also that poleward of the forcing regions there is strong southerly flow. The flow for u/t is almost constant with respect to xt except near the boundary where u has to come to zero. The theory so far illustrates how a strong boundary current can be set up but is unrealistic to the extent that there is no mechanism to stop the buildup of the long-shore flow. We will now consider how the quadratic increase with time of the northward boundary flow can be stopped. Dissipative processes slow down the buildup of the long-shore velocity and permit a steady state to be achieved in which the width of the jet is determined by K, the eddy diffusivity of momentum, and the source/sink strength.

c. *Steady-state dissipative solution*

In reality, the jet may be retarded by both lateral rubbing and by vertical friction, particularly with the ground. The latter will give rise to a vertical shear, which cannot be accommodated in this simple model. Such a frictional effect on the whole layer could be simulated by a Rayleigh friction term, but horizontal rubbing would appear to be the more important. The steady-state equations are

$$\left.\begin{aligned}-\tfrac{1}{2}yv&=-h_x+K(u_{xx}+u_{yy})\\ \tfrac{1}{2}yu&=-h_y+K(v_{xx}+v_{yy})\\ u_x+v_y&=Q\end{aligned}\right\}, \tag{24}$$

with solutions to these equations in the absence of boundaries and longitudinal source/sink inhomogeneities having already been found. Munk (1950) has shown that an equation for v follows from (24):

$$v_{xxxx}-\frac{v_x}{2K}+2v_{xxyy}+v_{yyyy}=\frac{y}{2K}Q_x+Q_{xxy}+Q_{yyy}. \tag{25}$$

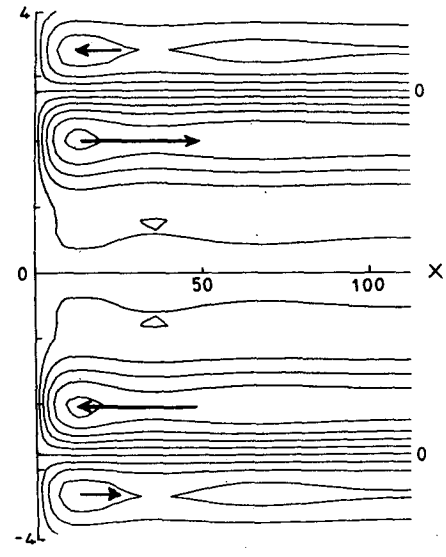

FIG. 5b. Contours of the asymptotic zonal velocity u/t in (y,xt) space, for the dynamic spin-up phase showing the strong east-west jets. The contour interval is 0.3.

In the boundary region, the x scale is usually smaller than the y scale so $\partial/\partial y$ is small compared to $\partial/\partial x$ and hence such terms will be dropped. Solutions of the homogeneous part of (25) are

$$v=e^{\gamma(x-L)},\quad e^{\alpha x},\quad e^{\beta x}, \tag{26}$$

where

$$\gamma=(\tfrac{1}{2}K)^{\frac{1}{2}},\quad \alpha=\gamma(-\tfrac{1}{2}+\sqrt{3}/2i),\quad \beta=\gamma(-\tfrac{1}{2}-\sqrt{3}/2i),$$

and L is the width of the basin in the x direction. Thus the solution for v is of the form

$$v=A(y)e^{\alpha x}+B(y)e^{\beta x}+C(y)e^{\gamma(x-L)}+v_I,$$

where v_I is the interior solution, which for small K, will be the solution of

$$\left.\begin{aligned} -\tfrac{1}{2}yv&=-h_x\\ \tfrac{1}{2}yu&=-h_y\\ u_x+v_y&=Q \end{aligned}\right\}, \tag{27}$$

i.e.,

$$\left.\begin{aligned} v_I&=-yQ\\ p_I&=-\tfrac{1}{2}y^2Q(y)x+\varphi(y)\\ u_I&=U_0(y)+(2Q+yQy)x \end{aligned}\right\}, \tag{28}$$

where $\partial\varphi/\partial y=-\frac{1}{2}yU_0(y)$. At the eastern boundary, only one term is available to satisfy $v=0$, i.e., $C(y)$. Thus, no control is possible over u, which must be solved for from (28). At $x=L$, $U_I=0$ implying $U_0(y)=-(2Q+yQ_y)L$ and hence to within an irrelevant constant in the pressure field, the eastern and interior solutions are determined. The form of $A(y)$ and $B(y)$ are obtained by applying the boundary conditions $u=0$, $v=0$ at $x=0$. The solution for v away from an eastern boundary is

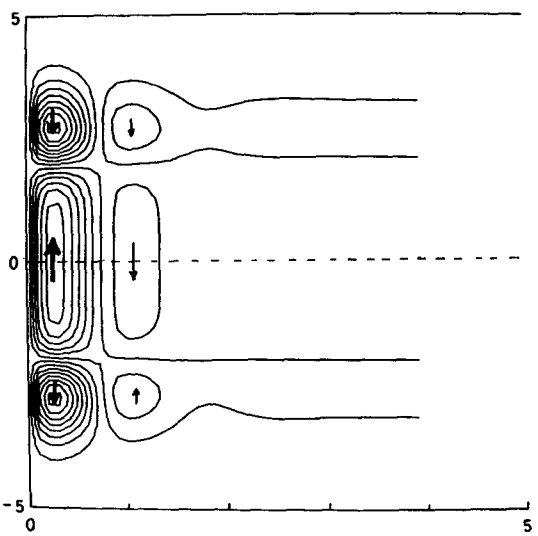

FIG. 6a. Contours of the v-field for the frictional solution (29) for forcing of the form (31) applied in the range $0<x<5$. The contour interval is 3.

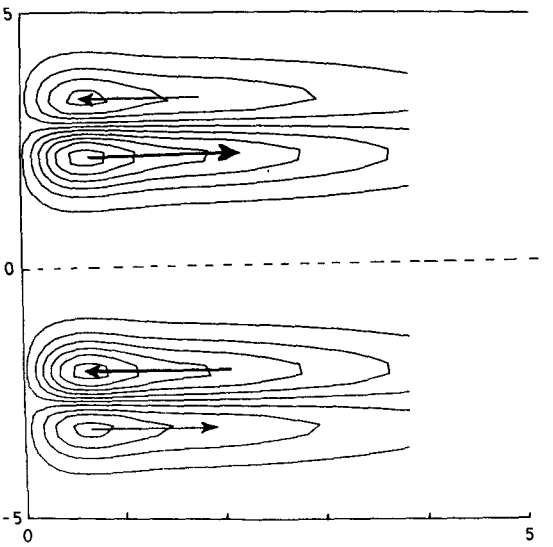

FIG. 6b. Contours of the u-field. The contour interval is 3.

$$v=e^{-\gamma x/2}\frac{2\gamma L}{\sqrt{3}}\left[\int_M^y(2Q+yQ')dy-\frac{yQ}{2\gamma L}\right]\sin\tfrac{1}{2}\sqrt{3}\gamma x$$
$$+yQ[e^{-\gamma x/2}\cos\tfrac{1}{2}\sqrt{3}\gamma x-1]. \tag{29}$$

For the problems considered here, v will be zero at $y=\pm M$ (rigid boundaries) but these boundaries are irrelevant as Q will be chosen to be nonzero only in a region well removed from them; hence there are no boundary currents at these walls. This solution is identical to that for the case $v\to 0$ as $y\to\pm\infty$. The second term in square brackets is small compared with the first since $\gamma\gg 1$, $L>1$, and hence could be dropped.

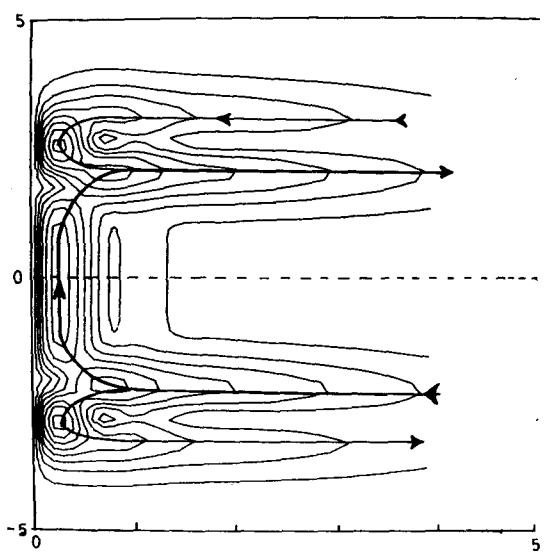

FIG. 6c. Contours of $w=(u^2+v^2)^{\frac{1}{2}}$. The contour interval is 3.

The solution for u corresponding to (29) is

$$u=(2Q+yQ')\times\left[(x-L)+\frac{L}{\sqrt{3}}e^{-\gamma x/2}(\sqrt{3}\cos\tfrac{1}{2}\gamma\sqrt{3}x+\sin\tfrac{1}{2}\gamma\sqrt{3}x)\right]. \quad (30)$$

The first term in Eq. (30) is the Sverdrup solution and the second is the boundary response. Comparison with (29) shows that the boundary response in v is $\sim\gamma$ larger than the corresponding response for u, but that the interior solution for u can be much larger than the interior solution for v. The Sverdrup solution near the western boundary increases as L increases. However, if we consider the forcing to span only the region $0<x<L$ and to be zero for $x>L$, then the solution (29) and (30) can be shown to apply to a channel of semi-infinite length. [Integration of (27) shows that the Sverdrup solution starts at $x=L$ and builds up linearly only in the region $0<x<L$ and is zero for $x>L$. Since the north-south flux contained in boundary layers near $x=L$ is negligibly small for small K, no significant effects are experienced in the interior or near the western boundary.]

The solutions of (29) and (30) are shown in Figs. 6a and 6b. The scalar wind $w=(u^2+v^2)^{\frac{1}{2}}$ is shown in Fig. 6c. The forcing used is of the form

$$Q=-\exp[-1.5(y-y_0)^2]+\exp[-1.5(y+y_0)^2], \quad y_0=2.5, \quad (31)$$

applied in the range $0<x<5$. The meridional velocity field shows a coastal jet flowing northward across the equator as expected, but to the north and south, as for the dynamic spin-up problem of Section 2b, there are again regions of southward flow. The east-west velocity shows a shear line at $y\approx 2.75$, i.e., poleward of the position of maximum forcing ($y=2.5$). Fig. 6c, for the scalar wind, shows a fair resemblence to the observed jet axis profile (cf., Fig. 1). Indeed in Fig. 1 of Findlater (1974) there is a suspicion of the equatorward flow feeding into the westerly jet maximum which is clearly shown in Fig. 6c. The fact that the jet maximum occurs *not while the current is hugging the boundary but after it has broken away from the boundary region* is in good agreement with the observational results. However, there are important differences; Fig. 1 shows that the flow is not symmetric with respect to the equator. This can result from nonlinear effects (see Section 3), land-sea contrasts (not considered), or zonal or meridional asymmetries in the forcing (considered below).

When the forcing is restricted to the region $N<x<L$, this solution is approximately

$$\left.\begin{aligned} v&=\frac{2\gamma(L-N)}{\sqrt{3}}e^{-\gamma x/2}\sin\tfrac{1}{2}\sqrt{3}\gamma x\int_M^y(2Q+yQ')dy\\ u&=(2Q+yQ')\left[-(L-N)+\frac{(L-N)}{\sqrt{3}}e^{-\gamma x/2}(\sqrt{3}\cos\tfrac{1}{2}\sqrt{3}\gamma x+\sin\tfrac{1}{2}\sqrt{3}\gamma x)\right]\end{aligned}\right\}, \quad 0<x<N, \quad (32a)$$

$$\left.\begin{aligned} v&=-yQ\\ u&=(2Q+yQ')(x-L)\end{aligned}\right\}, \quad N<x<L, \quad (32b)$$

$$\left.\begin{aligned} v&=0\\ u&=0\end{aligned}\right\}, \quad x>L. \quad (32c)$$

For the case $L=5$, $N=2$, the scalar wind is plotted in Fig. 7a for forcing of Eq. (31) and in Fig. 7b for forcing of the form

$$Q=-\frac{\exp[-0.5(y-y_0)^2]}{\sqrt{3}}+\exp[-1.5(y+y_0)^2], \quad y_0=2.5. \quad (33)$$

In all cases, a region of strong southward flow poleward of the cross-equatorial jet is present. This flow exists, as a boundary layer is needed to transport the large zonal fluxes equatorward of the forcing region across the shear layer, to allow part of them to be returned in the flow on the poleward side. It is thus of interest to examine the sensitivity of the north-south and east-west flows to various types of source/sink distributions.

It is also of interest to compare these profiles with those for the spin-up problem considered in Section 2b. For the forcing of Eq. (31) with $y_0=1.5$, 2.5, the meridional velocity profiles at $x=0$ are plotted in Fig. 8a for the inviscid dynamic spin-up case (curves D1.5, D2.5) and at the longitude of the southerly jet maximum for the frictional case (F1.5, F2.5). As shown later curve L2.5 is the solution obtained by integrating Eq. (37). The solutions are qualitatively similar but in the frictional case the solution tends to be less y dependent for small y and also the position of the northerly jet max appears to be more sensitive to changes in the source distribution. This is most easily illustrated for a step function source distribution of the form

$$Q=H(y-b)-H(y-a). \quad (34)$$

Then the form of v for the frictional solution is given by

$$v=\int_{-\infty}^{y} Q\partial y+yQ\Big]_{-\infty}^{y}, \tag{35}$$

whose solution is

$$\left.\begin{aligned} v&=0, && y<b\\ v&=(2y-b), && b<y<a\\ v&=a-b, && a<y<0 \end{aligned}\right\}. \tag{36}$$

This solution is plotted in Fig. 8b, and the dynamic solution (22) is also plotted for the case $b=-3$, $a=-2.3$

This illustrates the rule that while the velocity equatorward of the main forcing region will be positive, it will be negative within at least part of the forcing region, and the further the forcing region is from the equator, the more negative it is. Thus it is not hard to produce southward flow which is much stronger than northward flow near $y=0$ (see Fig. 6a). However, as Figs. 6b, 7a and 7b show, strong east-west shear lines can develop. In the previous analysis, y gradient dissipation was ignored. This will act to smear out the shear lines in u, which will in turn reduce the need for the north-south boundary current to return this flow across the shear line. This implies that the regions of strong southerly flow will be greatly reduced when y momentum is mixed. The following section gives the results of numerical experiments designed to test this, the importance of nonlinearity, the consequences of having a nonstationary sink region, and longitudinal spatial inhomogeneities in the source/sink distribution.

3. Results of numerical experiments

A series of numerical experiments (A–F) was performed to test the sensitivity of results to the various

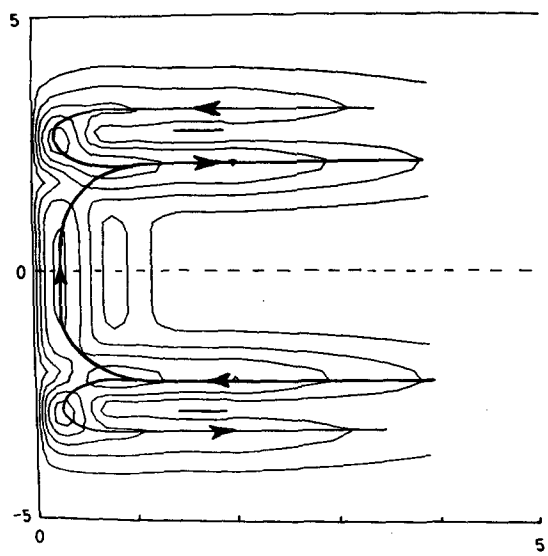

FIG. 7a. Contours of $w=(u^2+v^2)^{\frac{1}{2}}$ for forcing of the form (31) applied in the range $2<x<5$. The contour interval is 3.

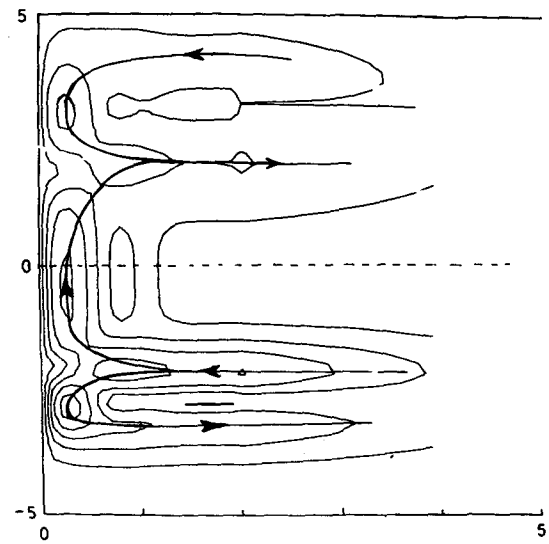

FIG. 7b. As in Fig. 7a with forcing of the form (33).

factors listed at the end of Section 2c. The nonlinear equations used are

$$\left.\begin{aligned} u_t&=-uu_x-vu_y+\tfrac{1}{2}yv-h_x+K(u_{xx}+u_{yy})\\ v_t&=-uv_x-vv_y-\tfrac{1}{2}yu-h_y+K(v_{xx}+v_{yy})\\ h_t&=-(hu)_x-(hv)_y+Q \end{aligned}\right\}. \tag{37}$$

In experiments A–F, the fluid is contained in a square box of length 10 units, symmetrically placed with respect to the equator. At the zonal boundaries, $y=\pm 5$, $u_y=v=0$, while at the meridional boundaries $x=0$, 10, $u=v=0$. Strictly speaking, the modal-type analysis used in Section 2 to introduce reduced gravity g' and effective depth H, cannot be performed when the equations are nonlinear, but qualitatively, inertial effects can be studied by generalizing (3) to (37). The geometrical distribution of sources and sinks to be used is shown in Fig. 9.

a. Experiment A

In Section 2c viscous solutions for the linear problem were obtained under the assumption that x derivatives were more important than y derivatives. On this basis Figs. 6a–c were produced; however they show regions of strong northerly flow in the boundary layer, poleward of the main cross-equatorial jet. These northerlies are likely to be reduced if y momentum is mixed. The first experiment was designed to test this and compare results with the analytical solution. Forcing of the form (31) was used in the range $0<x<8$ with amplitude 0.00625. For this experiment the linearized forms of (37) were used. The northward velocity in the boundary layer is plotted in Fig. 8a as curve L2.5. Comparison of curves F2.5 and L2.5 shows that the northerly flow is significantly reduced in amplitude while the northward flow is much less affected. When the cross-equatorial

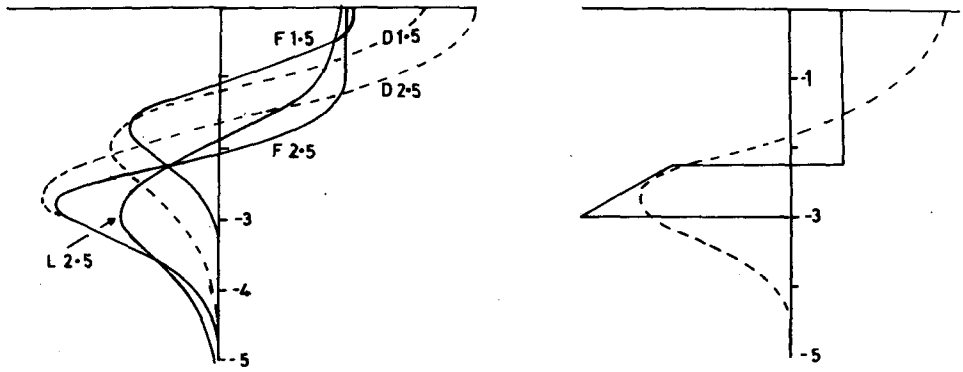

(a) (b)

FIG. 8a. The viscous solutions for v [Eq. (29)] as a function of y at the position of the maximum boundary current when forcing is of the form (31) with $y_0=1.5$, 2.5 (curves F1.5, F2.5 respectively). The inviscid dynamic spin-up solutions [Eq. (22)] are plotted for comparison (D1.5, D2.5). Curve L2.5 is the solution to the linear numerical model of Section 3 (experiment A).

FIG. 8b. The viscous (solid) and inviscid solutions (dashed) in the range $-5<y<0$ for forcing of the form $Q=-H(y+2.3)+H(y+3)$ showing how the frictional solution can have larger northerly boundary jets, with a less intense northward jet. The scale of the horizontal axis is arbitrary. Note that the frictional solution is steady, while the dynamic solution increases quadratically with time.

flow is plotted as a function of x from the solution (29) and compared with the numerically predicted values, the agreement is very good, illustrating that the solution (29) is generally acceptable. In Fig. 10, $w=(u^2+v^2)^{\frac{1}{2}}$ for the frictional solution of experiment A is plotted for comparison with Fig. 6c. The results are very similar except that, as expected, the regions of strong northerly flow are now considerably weaker.

b. Experiment B

To test the importance of nonlinearity, experiment B was run for the same configuration as A, but using Eqs. (37). The form of the forcing used is

$$Q=-0.00625\exp[-1.5(y-y_0)^2 + 0.00625\exp[-1.5(y+y_0)^2]. \quad (38)$$

In Fig. 11 velocity vectors are plotted. The solution is now strongly asymmetric, with the region of strongest flow well into the Northern Hemisphere, a result which seems to be in agreement with observation (cf. Fig. 1a). In the linear case, parity is conserved and an antisymmetric Q field will produce a symmetric v field, but in the nonlinear case, this parity is not conserved, and the velocity maximum is advected by the mean flow. (A symmetric Q field, however, will produce an antisymmetric v field even in the nonlinear case, for parity is conserved in this case.) In Fig. 12, the v field is plotted at four times, showing the northward movement of the velocity maximum. A phenomenon similar to this has also been observed by Cox (1976) in a much more complicated model of the Somali ocean current when his model is forced by a cross-equatorial wind stress. There, the upwelling zone moves northward in the same manner as the velocity maximum does here.

c. Experiment C

This is the same as B but with the source/sink strength doubled. Comparing Fig. 13 for experiment C with Fig. 11, one sees that increased nonlinearity has not moved the velocity maximum any further north, because such movement is blocked by the forcing which is at a fixed latitude. Of more interest is the fact that the velocity maximum of the zonal velocity is pushed away from the coast. Also, the weak southerly flow which occurs to the east of the main northward flow occurs much further from the boundary in experiment C then in experiment B. There is no evidence in the observations in Fig. 1b for any southerly flow near the jet maximum. Comparison of the results of experiments A, B and C, however, show that nonlinear effects push this weak southerly flow region poleward and eastward, which apparently is more in accord with observation.

d. Experiment D

While the source region of the Southern Hemisphere high pressure belt spans a broad band of latitude right up to the meridional African mountain chain, the sink region is more likely to be concentrated over India which is well removed from the meridional boundary. To simulate this, the sink region of experiment B is restricted to $4\leqslant x\leqslant 8$ but to conserve the total fluid mass, the sink strength is doubled. The results are shown in Fig. 14. By comparing this with Fig. 11, we see that in the Northern Hemisphere the region of strongest zonal flow is much more extensive in this case than in experiment B. This results from the way the Sverdrup solution for u is set up and can easily be explained from the linear results of Section 2c. Making

the sink region remote from the boundary does not allow the boundary jet to penetrate any further north, however. This result is in accord with the linear theory of Section 2c [cf. Eqs. (29) and (32)] but one might have expected some inertial overshoot in the boundary current (Bryan, 1963), since in this experiment there is no local sink to block the northward flow in this region.

e. Experiment E

The *Meteorological Atlas of the International Indian Ocean Experiment* (Ramage *et al.*, 1972) shows that there is a region of low-level convergence near the equator even during the southwest monsoon. To simulate this, a sink region spanning the equator was included between $x=4$ and $x=8$. The forcing used was of the form

$$Q=\begin{cases} 0.00625\exp[-1.5(y+y_0)^2], & 0<x\leqslant 8 \\ -0.00625\exp[-1.5(y+y_0)^2], & 4<x\leqslant 8 \\ -0.00625\exp[-1.5y^2], & 4<x\leqslant 8 \end{cases} \quad (39)$$

with $y_0=2.5$.

The results are shown in Fig. 15. Comparison with Fig. 14 shows that the equatorial sink leads to the

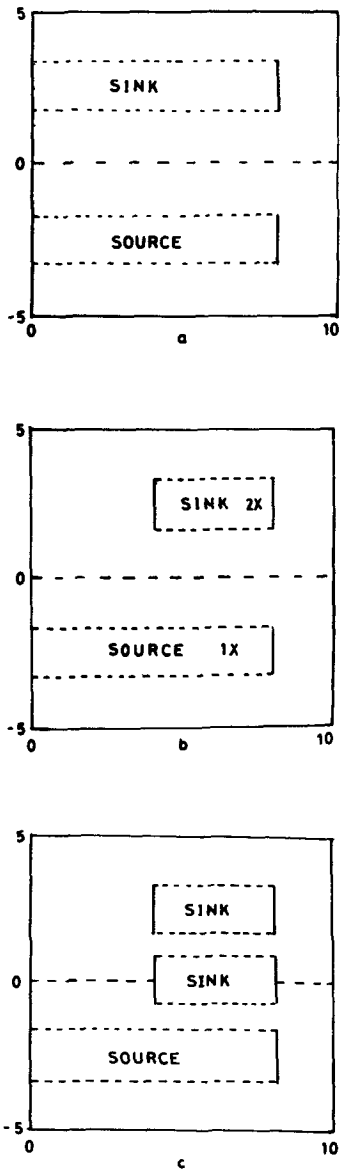

FIG. 9. Geometric configuration of the source/sink distributions used in experiments A–G. Distribution a is used for experiments A, B and C, b for D and F, and c is used for experiment F. The source/sink profile is Gaussian in the y direction and dashed lines indicate where this profile attains a value of $1/e$ relative to the maximum.

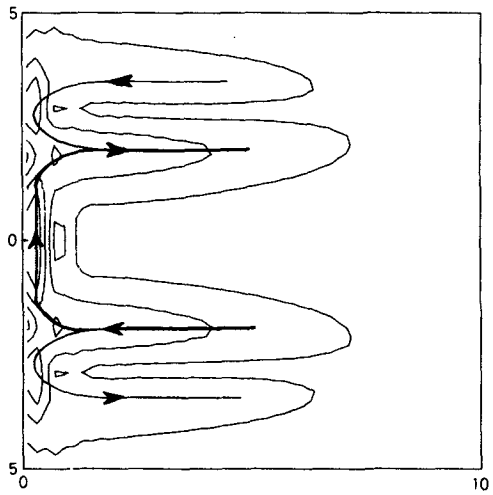

FIG. 10. Contours of $w=(u^2+v^2)^{\frac{1}{2}}$ for experiment A, for comparison with Fig. 6c. Contour interval is 0.04.

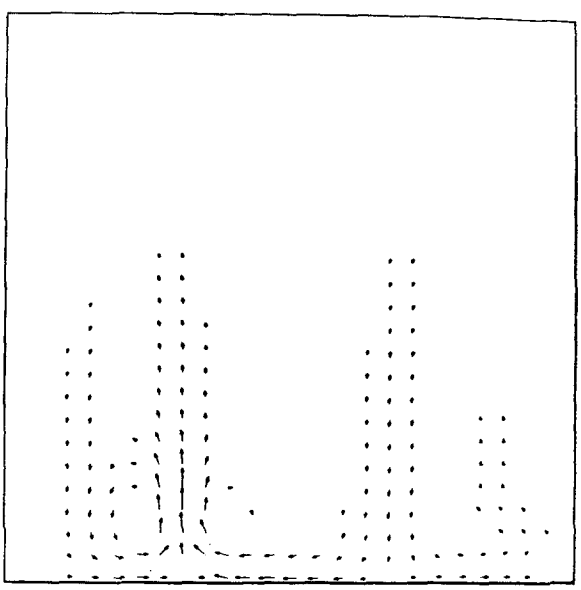

FIG. 11. Velocity for experiment B. An arrow the length of the grid interval Δ represents a nondimensional velocity of magnitude 0.22. Time=90 nondimensional units.

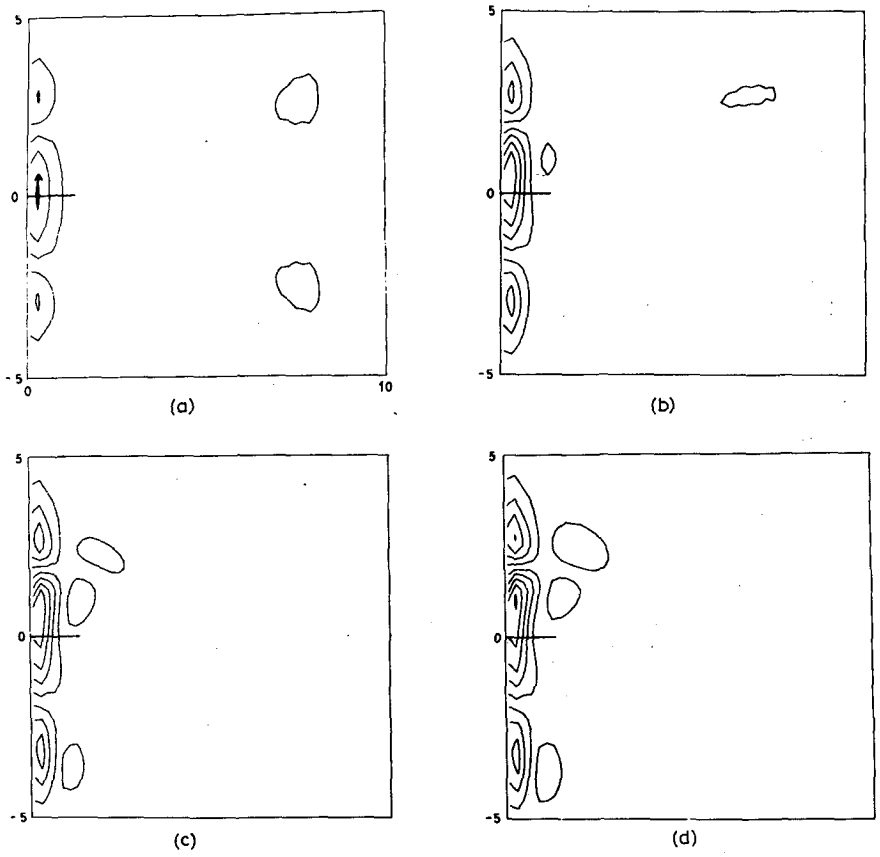

FIG. 12. Contours of v at dimensionless times 18, 36, 54, 72 (a–d) for experiment B, showing the northward displacement of the velocity maximum due to inertial effects.

formation of a standing eddy to the east of the boundary jet and a weakening of the zonal flow south of the heat low. It also emphasizes the fact that the intuitive idea that flow emerging from the Southern Hemisphere high pressure belt well to the east of the boundary would be sucked into the equatorial sink region is not true. Instead, a north-south pressure gradient is set up, which forces the air into an easterly jet. Cross-equatorial flow takes place only in the western boundary current and the equatorial sink induces only a weak westerly airstream along the equator.

f. Experiment F

Findlater (1974) reports that the jet can often be much stronger than the monthly mean strength. From observations of rainfall it is clear that the monsoon over India is not a continuous event. It thus seems plausible that variations in the intensity of the jet may be related to variability in the low-level convergence over India, and Findlater (1969) finds such a relationship. To simulate this, and to examine the sensitivity of the low-level jet to variations in the strength of the monsoon convergence[3] forcing of the form

$$Q=\begin{cases} 0.00625\exp[-1.5(y+y_0)^2], & 0<x\leqslant 8 \\ -0.0125\exp[-1.5(y-y_0)^2](1-\cos\omega t), & 4<x\leqslant 8 \end{cases} \tag{40}$$

for $y_0=2.5$, $\omega=2\pi/72$, was used. Spatially, the distribution is as for experiment D. Observationally, the forcing has a period of $\sim$10 days (Walker, 1972). The value of K used in the above experiments was 0.005, a value which gives the maximum poleward flow at the equator at 0.3 nondimensional units from the boundary (corresponding to 3°) a value in fair accord with Fig. 1b. This value of K is such that it takes $\sim$20 days for a steady frictional spin-up solution to be achieved (as in experiments A–E). This implies the 10-day oscillation is of too high a frequency to produce any significant effect.

[3] Findlater (1969) suggests that it may be the jet which induces variations in the monsoon. With this simple model it is not possible to examine this aspect. However, the result that variations in the strength of the jet over Kenya precede variations in rainfall is disputed by Raghavan *et al.* (1975).

If the period were increased to 24 days (or alternatively the value of K halved), then a more significant effect is likely. (Reducing K by a factor of 2 has a small effect on the boundary layer width because this is proportional to $K^{\frac{1}{2}}$.) It is more convenient to keep K at 0.005 but to increase the period of the forcing to 24 days. The results are shown in Fig. 16. These graphs show that there is not only a local response to the oscillating sink but that significant changes occur even in the Southern Hemisphere flow. The strength of the boundary current shows variations of up to 30% and the position of the maximum velocity of the boundary current shifts significantly, though it is in the zonal flow of the Northern Hemisphere that the strongest flow variations take place. The direction of the streamlines in the vicinity of the sink is also interesting. Comparison with Fig. 14, experiment D (which has the same geometrical configuration) shows that for a steady sink the streamlines have only very weak curvature. There is a phase lag between the sink and the intensity of the associated zonal jet.

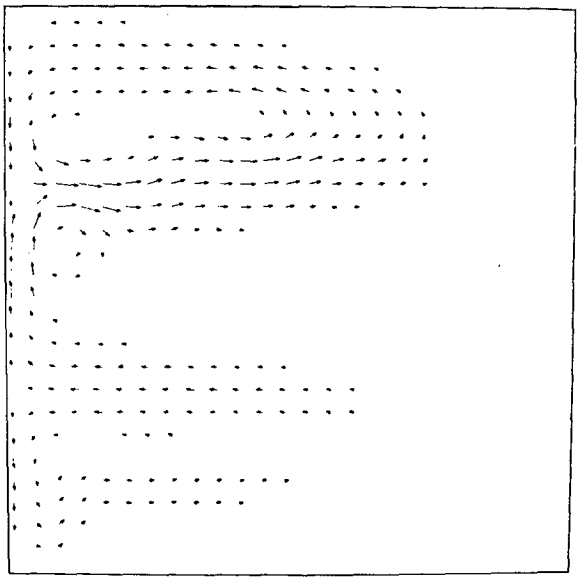

FIG. 14. Velocity vectors for experiment D (see Fig. 9) where the sink strength is double that of B but only half as extensive. $\Delta=0.18$. Time=90 nondimensional units.

g. *Experiment* G

The mountain chain running roughly north-south up the east African continent has an offshoot at $\sim 10°$N where the Ethiopian highlands branch off eastward into the Somali Republic. To analyze the effect of these mountains on the flow, the geometry was altered to that in Fig. 17 with a source/sink distribution similar to experiment D (Fig. 14). The velocities are remarkably similar. The east-west barrier acts mainly to increase the strength of the reverse flow east of the jet, i.e., it tends to set up a standing eddy. As experiments A–F show, the Ethiopian-Somali mountain chain is not required to produce a separation of the low-level jet from the boundary.

4. Summary

A simple one-layer model of the low-level jet has been proposed, forced by a source region simulating the low-

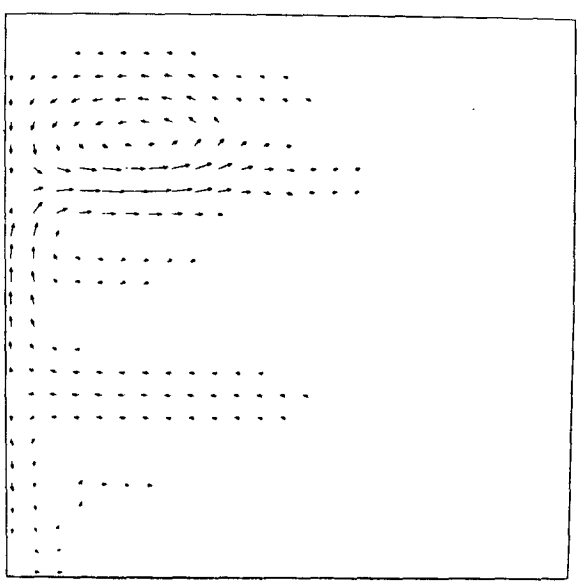

FIG. 13. Velocity vectors for experiment C. The forcing is double that of B and while the zonal jet in the Northern Hemisphere is more intense and extensive the latitude of the jet max is unaltered. $\Delta=0.44$. Time=90 nondimensional units.

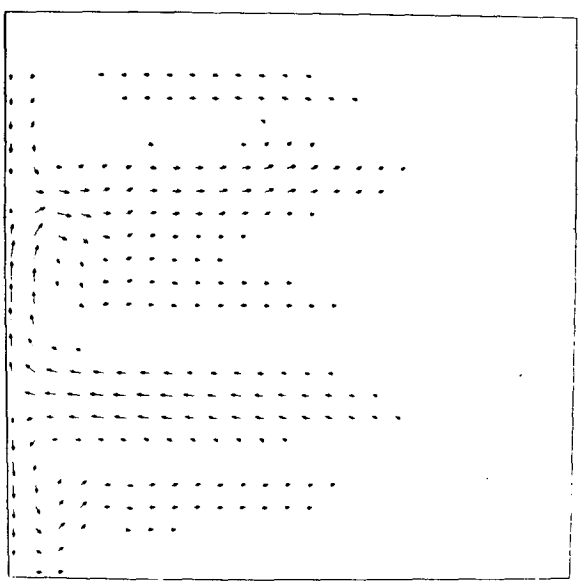

FIG. 15. Velocity vectors for experiment E for which a sink region along the equator has been included. This sink does not induce any cross-equatorial flow downstream of the boundary but does induce a standing wave east of the boundary current. $\Delta=0.14$. Time=90 nondimensional units.

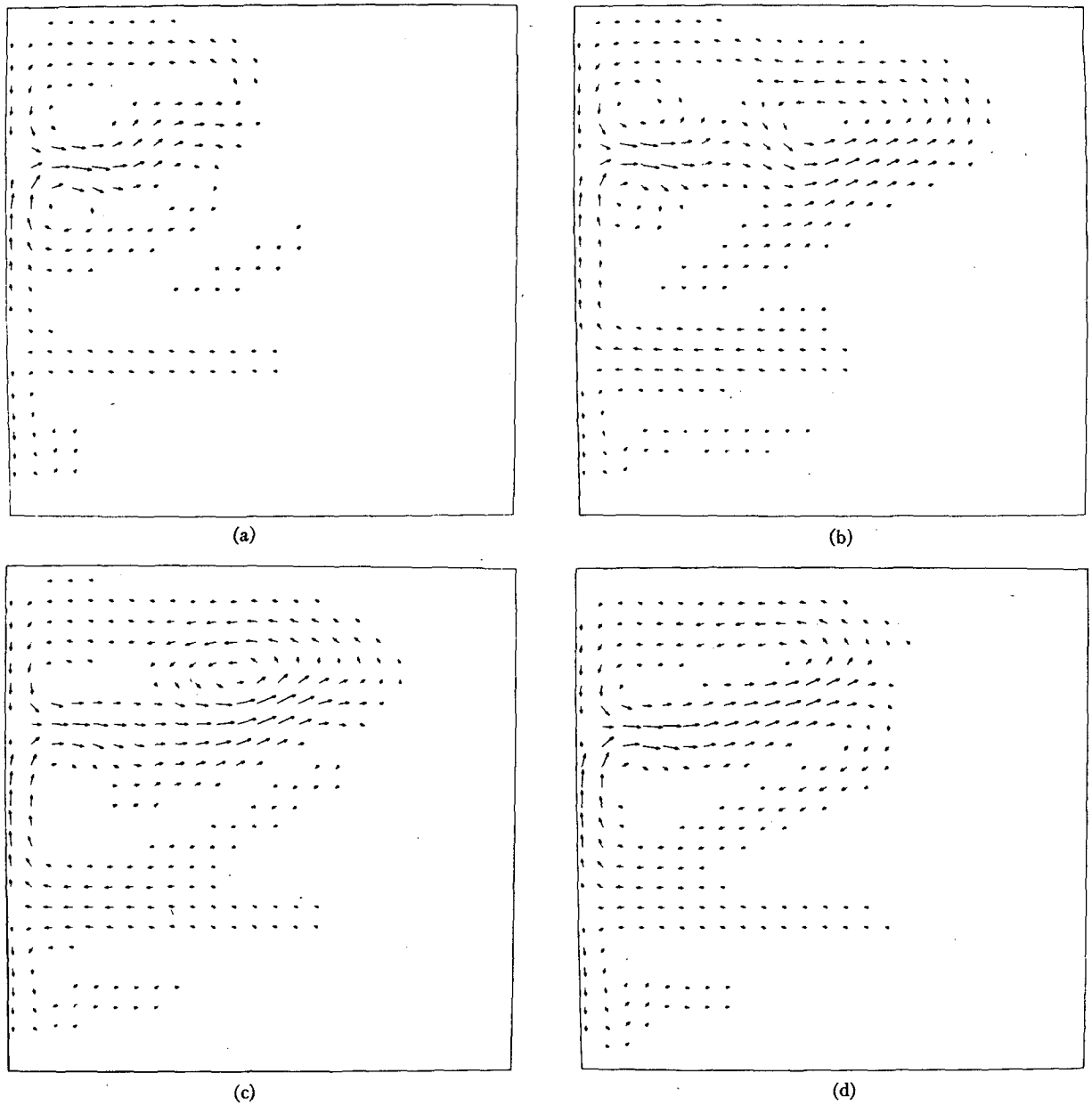

FIG. 16. Velocity vectors for experiment F when the sink region is oscillatory, at dimensionless times 90, 108, 126, 144 (a–d). Strong flow changes are induced which are not entirely localized. The period of the forcing is 72 units of dimensionless time. Δ has the values 0.24, 0.20, 0.22, 0.22, respectively, for a, b, c, d.

level divergence of the Southern Hemisphere high pressure belt and a sink region simulating the convergence of the monsoon trough. In Section 2a, solutions in the absence of a mountain chain are obtained, and then in 2b the dynamic method by which a boundary current is formed when a mountain barrier is present is examined. It is shown how long and short planetary waves give rise to a cross-equatorial jet. In the inviscid case, velocities in the boundary jet intensify quadratically with time. This implies that viscous and nonlinear effects become important. From observations the jet has both strong lateral and vertical shears implying both horizontal and vertical eddy momentum transfers. The vertical shear cannot be simulated with this crude model so only horizontal mixing is included, and in Section 2c simplified analytic solutions for u and v are obtained for various distributions of sources and sinks. These solutions give results which are in general qualitatively similar to the observed structure but are unrealistic in that they suggest that there is a reverse cross-equatorial flow just to the east of the northward jet. Subsequent nonlinear numerical experiments

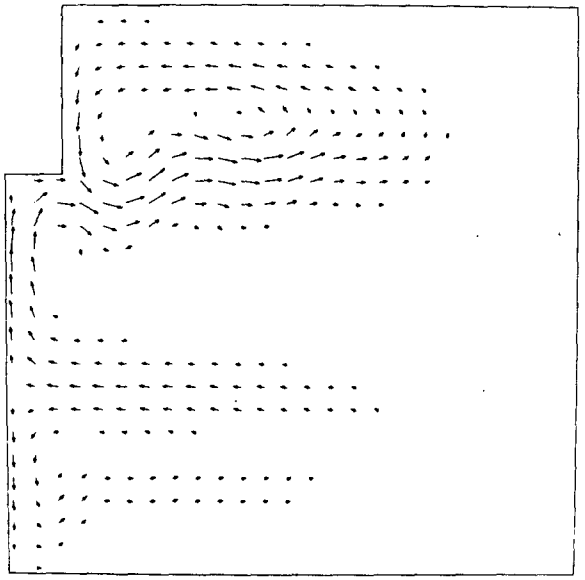

FIG. 17. Velocity vectors for experiment G when the western boundary is indented. This indentation is not required to produce a separation of the low-level jet from the boundary but does appear to amplify a standing wave east of the jet. $\Delta=0.16$. Time=90 nondimensional units.

showed that this reverse flow is weakened and displaced northward and eastward by inertial effects. Inertial effects also displace the jet maximum northward. When the sink region is made to vary with time it becomes apparent that significant changes can be induced in the flow pattern even in the opposite hemisphere, that the position of the northerly jet maximum is strongly affected, and that the westerly jet close to the sink undergoes orientation changes as well as variations in intensity. This may be related to the temporal variations in the cross-equatorial jet observed by Findlater.

Acknowledgments. This work arose from a chance meeting with Suki Manabe, and his helpful thoughts are acknowledged. Peter Killworth's advice with respect to Section 2c is also acknowledged.

REFERENCES

Anderson, D. L. T., and A. E. Gill, 1975: Spin-up of a stratified ocean with applications to upwelling, *Deep-Sea Res.*, **22**, 583–596.

——, and P. B. Rowlands, 1976a: The role of inertia-gravity and planetary waves in the response of a tropical ocean to the incidence of an equatorial Kelvin wave on a meridional boundary. *J. Marine Res.* (to be published).

——, and ——, 1976b: The Somali Current response to the southwest monsoon: The relative importance of local and remote forcing. *J. Marine Res.* (to be published).

Bryan, K., 1963: A numerical investigation of a nonlinear model of a wind driven ocean. *J. Atmos. Sci.*, **20**, 594–606.

Cox, M. J., 1976: Equatorially trapped waves and the generation of the Somali Current. *Deep-Sea Res.* (to be published).

Findlater, J., 1969: A major low-level air current near the Indian Ocean during the northern summer. *Quart. J. Roy. Meteor. Soc.*, **95**, 362–380.

——, 1974: The low-level, cross-equatorial air current of the western Indian Ocean during the northern summer. *Weather*, **29**, 411–416.

Gill, A. E., and A. J. Clarke, 1974: Wind-induced upwelling, coastal currents and sea-level changes. *Deep-Sea Res.*, **21**, 325–345.

Hahn, D. G., and S. Manabe, 1975: The role of mountains in the South Asian monsoon circulation. *J. Atmos. Sci.*, **32**, 1515–1541.

Hide, R., 1968: On source-sink flows in a rotating fluid. *J. Fluid Mech.*, **32**, 737–764.

Lighthill, M. J., 1969: Dynamic response of the Indian Ocean to onset of the southwest monsoon. *Phil. Trans. Roy. Soc. London*, **265A**, 45–92.

Munk, W. H., 1950: On the wind driven ocean circulation. *J. Meteor.*, **7**, 79–93.

Newton, C. W., 1959: Synoptic comparison of Gulf Stream and jet stream systems. *The Atmosphere and the Sea in Motion*, B. Bolin, Ed., Rockefeller Institute Press, 288–304.

Raghavan, K., D. R. Sikka and S. V. Gujar, 1975: The influence of cross-equatorial flow over Kenya on the rainfall of western India. *Quart. J. Roy. Meteor. Soc.*, **101**, 1003–1005.

Ramage, C. S., F. R. Miller, and C. Jeffries, 1972: *Meteorological Atlas of the International Indian Ocean Expedition.* Washington, D. C., National Science Foundation.

Rao, Y. P., 1964: Inter-hemispheric circulation. *Quart. J. Roy. Meteor. Soc.*, **90**, 191–194.

Stommel H., 1948: The westward intensification of wind-driven ocean currents. *Trans. Amer. Geophys. Union*, **29**, 202–206.

Walker, J. M., 1972: The monsoon of Southern Asia: A review. *Weather*, **27**, 178–189.

Wexler, H., 1961: A boundary layer interpretation of the low-level jet. Tellus **13**, 368–378.